



HAL
open science

Three-dimensional Printing of Biomimetic Titanium Mimicking Trabecular Bone Induces Human Mesenchymal Stem Cell Proliferation

Stephanos Papaefstathiou, Nathanaël Larochette, Rosa María Villar Liste,
Esther Potier, Herve Petite, Bradley Vivace, Joseph Laratta

► **To cite this version:**

Stephanos Papaefstathiou, Nathanaël Larochette, Rosa María Villar Liste, Esther Potier, Herve Petite, et al.. Three-dimensional Printing of Biomimetic Titanium Mimicking Trabecular Bone Induces Human Mesenchymal Stem Cell Proliferation. *Spine*, 2022, 47 (14), pp.1027-1035. 10.1097/BRS.0000000000004317 . hal-03836586

HAL Id: hal-03836586

<https://hal.science/hal-03836586>

Submitted on 8 Nov 2022

HAL is a multi-disciplinary open access archive for the deposit and dissemination of scientific research documents, whether they are published or not. The documents may come from teaching and research institutions in France or abroad, or from public or private research centers.

L'archive ouverte pluridisciplinaire **HAL**, est destinée au dépôt et à la diffusion de documents scientifiques de niveau recherche, publiés ou non, émanant des établissements d'enseignement et de recherche français ou étrangers, des laboratoires publics ou privés.

Three-dimensional printing of biomimetic titanium mimicking trabecular bone induces human mesenchymal stem cell proliferation - An *in vitro* analysis

Authors : Stephanos PAPAEFSTATHIOU ^{1,2}, Nathanael LAROCLETTE ^{1,2}, Rosa Maria VILLAR LISTE ³, Esther POTIER ^{1,2}, Hervé PETITE ^{1,2}, Bradley J. VIVACE ^{4,6}, Joseph L LARATTA ⁵

Affiliations:

1. Université de Paris, CNRS, INSERM, B3OA, Paris, France
2. Ecole Nationale Vétérinaire d'Alfort, B3OA, Maisons-Alfort, France
3. FIDIS. NEIRID Hospital Clínico, Santiago de Compostela, Spain
4. University of Louisville School of Medicine, Louisville, KY, USA
5. University of Louisville Department of Orthopedic Surgery, Louisville, KY, USA
6. University of Missouri Department of Orthopaedic Surgery, Columbia, MO, USA

Key words: 3D printing, additive manufacturing, fusion, intervertebral implant, porous, spine, titanium

To cite this article: Papaefstathiou S, Larochette N, Liste RMV, Potier E, Petite H, Vivace BJ, Laratta JL. Three-dimensional Printing of Biomimetic Titanium Mimicking Trabecular Bone Induces Human Mesenchymal Stem Cell Proliferation: An In-vitro Analysis. Spine (Phila Pa 1976). 2022 Jul 15;47(14):1027-1035. doi: 10.1097/BRS.0000000000004317. Epub 2021 Dec 21. PMID: 34935757.

Document Version: Accepted manuscript including changes made at the peer-review stage.

Abstract

STUDY DESIGN. *In vitro* analysis.

OBJECTIVE. The aim of this study was to assess the effect of three-dimensional (3D) printing of porous titanium on human mesenchymal stem cell (hMSC) adhesion, proliferation, and osteogenic differentiation.

SUMMARY OF BACKGROUND DATA. A proprietary implant using three-dimensional porous titanium (3D-pTi) that mimics trabecular bone structure, roughness, porosity, and modulus of elasticity was created (Ti-LIFE technology™, Spineart SA Switzerland). Such implants may possess osteoinductive properties augmenting fusion in addition to their structural advantages. However, the ability of 3D-pTi to affect *in vitro* cellular proliferation and osteogenic differentiation remains undefined.

METHODS. Disks of 3D-pTi with a porosity of 70% to 75% and pore size of 0.9 mm were produced using additive manufacturing technology. 2D Ti6Al4V (2D-Ti) and 2D polyetheretherketone (2D-PEEK) disks were prepared using standard manufacturing process. Tissue culture plastic (TCP) served as the control surface. All discs were characterized using 2D-microscopy, scanning electron microscopy (SEM), and x-ray micro-computed tomography. Forty thousand hMSCs were seeded on the disks and TCP and cultured for 42 days. hMSC morphology was assessed using environmental SEM and confocal imaging following phalloidin staining. hMSC proliferation was evaluated using DNA fluorescent assay. hMSC differentiation was assessed using RT-qPCR for genes involved in hMSC osteogenic differentiation and biochemical assays were performed for alkaline phosphatase activity (ALP) and calcium content.

RESULTS. 3D-pTi lead to a higher cell number as compared to 2D-Ti and 2D-PEEK at D21, D28 and D42. ALP activity of hMSCs seeded into 3D-pTi scaffolds was as high as or higher than that of hMSCs seeded onto TCP controls over all time points and consistently higher than that of hMSCs seeded onto 2D-Ti scaffolds. However, when ALP activity was normalized to protein content, no statistical differences were found between all scaffolds tested and TCP controls.

CONCLUSION. 3D-pTi provides a scaffold for bone formation that structurally mimics cancellous bone and improves hMSC adhesion and proliferation compared to 2D-Ti and PEEK.

Introduction

The first spinal fusion was performed in 1891 for the treatment of Pott disease¹. Several arthrodesis techniques have since been developed with increasing emphasis on anterior column support and interbody fusion. Numerous implant materials have been utilized including allografts, metals, plastics, and composites².

Titanium and polyetheretherketone (PEEK) are the most commonly used materials in interbody implants. Unfortunately, both have limitations. While titanium improves cellular adhesion and bioactivity compared to PEEK, it has been associated with subsidence and difficulty in assessing osseous fusion due to radiopacity³.

Novel additive manufacturing techniques have allowed for the production of titanium-based biomimetic structures aimed at improving osseointegration. However, the effect these alterations have upon cellular proliferation, adhesion, behavior, and gene expression is not entirely understood.

We sought to evaluate human mesenchymal stem cell (hMSC) adhesion, proliferation, and differentiation on scaffolds of three-dimensionally printed porous titanium (Ti6Al4V) (3D-pTi) designed to mimic the characteristics of trabecular bone (Ti-LIFE technology, Spineart SA, Geneva, Switzerland) compared to scaffolds of standard titanium (2D-Ti) and PEEK.

Materials and Methods

3D-pTi, 2D-Ti, and 2D-PEEK disks (Ø 11.5 mm, h = 2 mm) were manufactured and sterilized by Spineart. Tissue culture plastic (TCP) was utilized as control.

Scanning electron microscopy (SEM)

Images were acquired with a Zeiss Ultra55 scanning electron microscope (SEM), with a high-resolution Schottky thermal field emission gun, with an electron emission at 5 kV, and fitted with the UHR Gemini column.

Micro-computed tomography

3D-pTi scaffolds were imaged using micro-computed tomography (CT) at the following settings: pixel size = 12.5 µm; voltage = 80 kV; current = 100 µA; filter = copper/aluminum; rotation step = 0.3°; exposure = 2375 ms (Skyscan 1172; Bruker, Belgium). Images were reconstructed using NRecon software (v1.6.8.0; Bruker, Belgium) and visualized with DataViewer and CT-vox softwares (Bruker, Belgium).

Cells and cell culture

hMSCs were isolated from bone marrow discarded following routine surgery from four donors (5–22 years' old) with consent via Lariboisière hospital (Paris, France). These cells were expanded in alpha-Minimal Essential Medium Eagle (αMEM) with 10% fetal bovine serum and 1% penicillin/ streptomycin using a procedure adapted from literature reports⁴. hMSCs were characterized by cytofluorometry and differentiation assays. These cells were positive for CD90, CD73, and CD105 and negative for CD45. Their osteogenic, adipogenic, and chondrogenic differentiation potentials were validated using established methods⁴. Cells from the four donors were cultured under standard conditions (37°C, 5% CO₂, and 95% air). At 80% to 85% confluence, the cells were trypsinized and pooled at an equal ratio

of 1:4. Forty thousand hMSCs were loaded on the scaffolds in 150 µL of medium and left for 4 hours at 37°C. Afterward, 500 µL of identical medium was added. The cell culture medium was removed and replaced with 500 µL of Lonza hMSC osteogenic differentiation medium bullet kit following 24 hours. Medium changes were performed every 2 to 3 days.

Confocal laser microscopy

TCP controls and scaffolds were processed on days 7, 28, and 42. Upon harvesting, they were washed twice with PBS, fixed with 4% paraformaldehyde in phosphate buffered saline (PBS) at room temperature (RT) for 15 minutes, washed twice with PBS, maintained in 2% Triton in PBS at RT for 15 minutes, and then washed twice with PBS. TCP controls and scaffolds were then kept wet at 4°C until staining, confocal microscopy examination, and image acquisition. Upon image acquisition, TCP controls and scaffolds were first incubated in PBS at RT with diamidino-2-phenylindole (DAPI) (5 mg/mL) for 40 minutes, and then in ActinGreen 488 ReadyProbes Reagent at RT for 15 minutes, then washed three times with PBS. Images were acquired with TCP controls and scaffolds immersed in PBS on a Zeiss 780 upright laser scanning confocal microscope using λ 358 nm excitation and 1461 nm emission for DAPI and λ 495 nm excitation and λ 518 nm emission for ActinGreen.

Environmental SEM

TCP controls and scaffolds were processed on days 7, 28, and 42. Upon harvesting, the samples were washed twice with PBS, fixed using 2.5% glutaraldehyde in PBS at RT for 40 minutes, and washed twice with PBS. Images were acquired using a Philips XL30 ESEM FEG with a high-resolution Schottky thermal field emission gun, with an electron emission at 12 kV and a vapor environment of 3 to 5 Torr.

Proliferation

TCP controls and scaffolds were processed on days 0, 7, 14, 21, 28, and 42. TCP controls and scaffolds were washed with PBS and subsequently kept in 1 mL of CyQUANT lysis buffer at 37°C for 15 minutes, then stored at –20°C until specimens at all time points were collected.

All cell-quantification specimens were freeze-thawed 3 times. Each sample was immersed in liquid nitrogen for 30 seconds and thawed for 3 minutes in a 37°C water bath. Collagenase type II (3 mg/mL) was then added to each lysate sample and maintained at 37°C for 3 hours. Proteinase K (1 mg/mL) was added to each lysate and maintained at 37°C for 15 hours. These lysate samples were ultrasonicated in five cycles of 1" on/5" off using the Bioblock Scientific VibraCell ultra-sonicator (Sonic, Newtown, CT) set at 40 (1 Watt).

The cellular content in each lysate was determined using the CyQUANT cell proliferation assay kit. Upon the addition of the CyQUANT fluorescent dye, fluorometry was used to measure the lysate DNA content using a FL600 microplate fluorescence reader (BIO-TEK; Winooski, Vermont) at λ 485 nm excitation and λ 530 nm emission.

Calcium content assay

TCP controls and scaffolds were processed on days 28 and 42. Their calcium content was assessed by treating TCP control and each scaffold with 250 µL of 100 mmol/L hydrochloric acid at RT

for 2 hours. Following solubilization, the calcium content of the acid solution was determined using the bioMérieux Calcium content kit. Spectrometry values were acquired using the μ QUANT spectrophotometer (BIO-TEK) at λ 610 nm.

Alkaline phosphatase activity assay

TCP controls and scaffolds were processed on days 14, 21, 28, and 42. Cells on scaffolds and on TCP controls were harvested in alkaline phosphatase (ALP) lysis buffer and were treated with three freeze-thaw cycles and ultra-sonicated in five cycles of 1" on/5" off using the Bioblock Scientific VibraCell ultra-sonicator set at 40 (1 Watt), as previously described.⁵ Each 50 μ L aliquot of the cell lysate was treated with 250 μ L of 2-amino-2-methyl-1-propanol (AMP) buffer and 250 μ L of 4-nitrophenyl phosphate disodium salt hexahydrate (pnpp) and maintained at 37°C until the yellow coloration of p-nitrophenol (pnp) appeared. The chemical reaction was then stopped by the addition of 1 mL 0.1 mol/L sodium hydroxide. The ALP activity was then quantified via μ QUANT Biotek spectrophotometer at λ 410 nm. The spectrophotometry data were then converted to amount (μ mol) of pnp (resulting from the reaction of ALP and its substrate, pnpp) per time (the time taken for the appearance of the yellow coloration).

The protein content for each cell lysate was assessed using a BCA quantification assay (Pierce BCA protein assay), a standardized range of different albumin amounts, along with the samples, both treated with the colorimetric reagent of the kit, were heated at 37°C for 30 minutes. Absorbance readings were taken at λ 562 nm using the μ QUANT Biotek spectrophotometer.

Osteogenic gene expression

TCP controls and scaffolds were processed on days 0, 7, 14, 21, 28, and 42. Cells on scaffolds and TCP controls were lysed using TRIzol and were kept at -80°C until specimens at all time points were collected. At that time, chloroform was added to each trizolic extract to obtain a phase separation. The aqueous phase was then collected, the contained RNA was precipitated using isopropanol, washed with 70% ethanol, and re-suspended in nuclease-free water. The amount and integrity of the RNA preparation were assessed using the DS-11TM Series Spectrophotometer at λ 260 and 280 nm (Denovix; Wilmington, DE).

The RNA prep underwent reverse transcription using the SuperScript VILO cDNA synthesis kit in the iCycler (Biorad; Hercules, CA). The resulting cDNA was then used for realtime qPCR, using the TaqMan fluorescent probe system and the MyiQ cycler (Biorad). Before RT-qPCR testing, a representative pool of samples was used to determine the most suitable reference gene among three tested: 18S, GAPDH, TBP. 18S was selected as reference gene as it maintained the more consistent expression across all experimental conditions tested. Four osteogenic markers were used to assess hMSC osteo-differentiation: runt-related transcription factor 2 (RUNX2), integrin-binding sialoprotein (IBSP), bone gamma-carboxyglutamate protein (bGLAP), and osteopontin (also known as bone sialoprotein 1; SPP1).

Statistical methods

GraphPad Prism Software v6.01 (GraphPad Software, Inc) was utilized for statistical analysis. Data normality was tested with D'Agostino's test. For normally distributed data (DNA and calcium contents), one-way analysis of variance was utilized. When found significant, a Tukey post-hoc test was conducted. For non-

normally distributed data (ALP activity and osteogenic gene expression), Kruskal-Wallis test was utilized. When found significant, a Dun's test was conducted. For all analyses, differences at $P < 0.05$ were considered statistically significant.

Results

Scaffold morphology

Micro-CT images revealed the random, highly porous structure of the 3D-pTi scaffolds (Figure 1A and 1B). 2D-Ti and 2D-PEEK scaffolds displayed smooth surfaces with presence of grooves at higher magnification; 3D-pTi scaffolds showed a random textural geometry with titanium spherical deposits of various size and distribution (Figure 2).

hMSC morphology

Figure 3 shows confocal images of hMSCs seeded on the 3D-pTi scaffolds. At D7, hMSCs outlined the inner 3D-pTi structure in the central region of the scaffold where the hMSCs were initially seeded (Figure 3A and D). At D28, hMSCs were discernible in the outer "rim" of the 3D-pTi scaffold (left section of Figure 3B). hMSCs are comparatively less discernible at D42 (Figure 3C) due to the dense extracellular matrix (ECM). Dark circular bumps amidst the fluorescent phalloidin green either are the additively manufactured spherical deposits (Figure 3B, C, and F) or the struts of the 3D-pTi surface (Figure 3E and F). Actin stress fibers are also noticeable in Figure 3F.

Due to auto-fluorescence and reflectivity, only hMSCs seeded on 3D-pTi scaffolds were able to be visualized using confocal laser microscopy. Therefore, the seeded scaffolds were also imaged with environmental SEM.

At day 7 (A, D), day 28 (B, E), and day 42 (C, F), Figure 4 shows the environmental SEM images of hMSCs seeded on TCP controls and tested scaffolds (Figure 4). hMSCs seeded on TCP controls already displayed a dense layer at D7 and formed confluent multilayers at D21 and D28. For 2D-PEEK scaffolds, sparse cells were visualized at D7; hMSCs were able to proliferate and formed confluent multilayers similar to TCP controls at D42. hMSCs seeded on 2D-Ti showed a dense cell layer over all time points; however, in the majority of the 2D-Ti samples, hMSCs aggregated in the scaffold center to form a pellet that detached between D7 and D28. We theorize most hMSCs observed at D28 and D42 on these scaffolds are secondary cell growth originating from the few cells that remained adherent during the pellet aggregation. As for 3D-pTi scaffolds, hMSCs elongating in the 3D porous structure could be seen at D7. At D28 and D42, however, the layer formed was so dense it was impossible to distinguish hMSCs from the ECM they deposited. Notably, this confluent layer was observed in contact with the struts of the 3D structure and did not clog the pores of the 3D-pTi scaffolds, even after 42 days of culture.

hMSC proliferation

Regarding hMSC proliferation, no significant difference was found at D0 between the scaffolds and the TCP controls. At D7, 3D-pTi scaffolds showed a significant increase in cell number compared to 2D-Ti and 2D-PEEK scaffolds, similar to the TCP controls. The poor cell adhesion observed for 2D-PEEK using environmental SEM at D7 was confirmed with a lower cell number. 3D-pTi scaffolds confirmed their ability to lead to a higher cell

number as compared to 2D-Ti and 2D-PEEK scaffolds at D21, D28 and D42. At D42, the cell number on 3D-pTi scaffolds was significantly higher than observed in TCP controls (Figure 5A and B).

hMSC osteogenic differentiation

The highest upregulation of RUNX2, SPP1, and BGLAP gene expression levels over time were observed for the positive TCP controls (Figure 6A and B). Otherwise, no striking differences were observed between the different scaffolds. A slight upregulation of SPP1 gene expression levels was observed for 2D-Ti scaffolds at D28 and D42, as well as of IBSP gene expression levels for 2D-PEEK scaffolds at D21, D28, and D42.

ALP activity of hMSCs seeded into 3D-pTi scaffolds was as high as or higher than those seeded onto TCP controls (Figure 7A) over all time points. It was consistently higher than that of hMSCs seeded onto 2D-Ti scaffolds. This higher ALP activity may indicate a higher osteogenic differentiation of hMSCs seeded into 3D-pTi scaffolds. However, when ALP activity was normalized to protein content, no statistical differences were found between all scaffolds tested and TCP controls (Figure 7A–C).

3D-pTi scaffolds displayed calcium contents that were as high as TCP controls at D28 and D42, higher than 2D-Ti and 2D-PEEK scaffolds at D28, and higher than 2D-PEEK scaffolds at D42 (Figure 8A–C).

Discussion

Previous evidence demonstrated that osteointegration takes place due to several factors including topographical cues and chemical composition of the implant⁵⁻⁷. The roughness of the implant surface, its chemistry, topography, and wettability have been suggested to impact cellular properties⁸. Thus, manufacturing techniques that allow for enhanced implant bioactivity have been developed to augment osseointegration, including plasma sprays, composites, and hydroxyapatite-coatings². Recently, 3D printing has allowed for the production of titanium implants with porous and nanostructured topographies. In the present study, 3D-pTi designed to mimic trabecular bone was assessed *in vitro* for its effects on hMSC adhesion, proliferation, and differentiation.

hMSCs cultured on 3D-pTi displayed improved cellular adhesion, resistance to fragmentation, and density of colonization compared to 2D-Ti and 2D-PEEK scaffolds. Under SEM, there were mechanical perturbations in the hMSCs cytoskeleton suggestive of increased organelle transport noted in 3D-pTi scaffolds. Phalloidin staining revealed the development of a robust and organized highway of F-actin filaments in 3D-pTi hMSCs, which participate in the translation of mechanical forces experienced by the cell into biochemical/genetic changes in the nucleus. Interestingly, *ex vivo* loading of 3D printed spine implants have shown that these implants may macroscopically function in mechanotransduction responses as well⁹.

Regarding cellular proliferation, there was a significant increase in DNA content in the 3D-pTi compared to 2D-Ti and PEEK scaffolds at D7, D21, D28 and D42. hMSCs seeded on 3D-pTi surface also displayed a higher ALP activity as compared to 2D-Ti scaffolds at D14, D21, D28, and D42 and a higher calcium content as compared to 2D-PEEK scaffolds at D28, and D42. ALP activity is a marker of osteoblastic differentiation, maturation, bone formation, and bone matrix mineralization¹⁰. However, after

controlling for cell number, there was no significant increase in ALP activity. The increased ALP activity observed in the 3D-pTi scaffolds may be due to an increased number of cells rather than an improved osteogenic differentiation. Gene expression levels of RUNX2, bGLAP, and SPP1 were similar for all scaffold types, which corroborates the results of the ALP activity after controlling for cell number.

In a similar study using porous tantalum, increased hMSC proliferation and osteogenic gene expression was observed¹¹. Similarly, a study of titanium alloys reported increased expression of osteocalcin and osteoprotegerin¹². These results suggest that the metal composition, in addition to porosity and surface topography, may play a role in osteogenic activity/differentiation¹³. However, these reports did not compare the effects of commonly used materials in interbody fusion. In contrast, our report demonstrates the advantage of 3D-pTi over 2D-Ti and PEEK regarding cellular proliferation and adhesion.

In light of our findings, several limitations must be considered. The *in vitro* findings may not be generalizable to *in vivo* conditions. Furthermore, the clinical outcome of utilizing 3D-pTi cannot be ascertained and the trabecular structure may affect implant durability. Previous evidence suggests topography influences osteoblast behavior through integrin regulation; we did not evaluate this specific phenomenon and further study is necessary¹⁴. Furthermore, the ability of hMSCs to release trophic factors is established¹⁵, as such the inherent bioactivity of hMSCs may have impacted the results of our experiment and limit translatability to *in vivo* conditions; however, all scaffolds were tested with similarly sourced hMSCs in roughly equal initial quantities.

In conclusion, the structural alterations imparted by the 3D printing process upon the 3D-pTi scaffolds improved hMSC adhesion and proliferation compared to 2D-Ti and PEEK. The bioactivity and osteoconductive ability of titanium is significantly improved by the alterations imparted by 3D-printing, although further study is required to elucidate the putative mechanism for these findings given a lack of comparative upregulation of ALP or genes associated with osseous differentiation within the 3D-pTi scaffolds. Although *in vivo* studies and clinical trials are required to examine the effects of 3D-pTi on fusion and patient outcomes, it shows great promise in enhancing osseointegration.

Keypoints

- A proprietary 3D implant was created (Ti-LIFE technology, Spineart SA Switzerland) to mimic the characteristics of trabecular bone.
- Additive manufacturing techniques such as 3D printing purportedly augment the bioactivity of interbody implants while also optimizing their structure.
- We compared 3D titanium, 2D titanium, and polyetheretherketone scaffolds regarding *in vitro* human mesenchymal stem cell adhesion, proliferation, and osteogenic differentiation.
- 3D porous titanium scaffolds demonstrated improved human mesenchymal stem cell adhesion and proliferation.

Disclosure Statement

Spineart SA (Chemin du Pré-Fleuri 31228 Plan-Les-Ouates, Switzerland) funds were received in support of this work.

Relevant financial activities outside the submitted work: consultancy, royalties, travel/accommodations/meeting expenses.

References

1. Hadra BE. The classic: wiring of the vertebrae as a means of immobilization in fracture and Potts' disease. Berthold E. Hadra. *Med Times and Register*, Vol 22, May 23,1891. *Clin OrthopRelat Res* 1975;112:4–8.
2. Rao PJ, Pelletier MH, Walsh WR, et al. Spine interbody implants: material selection and modification, functionalization and bioactivation of surfaces to improve osseointegration. *Orthop Surg* 2014;6:81–9.
3. Chou YC, Chen DC, Hsieh WA, et al. Efficacy of anterior cervical fusion: comparison of titanium cages, polyetheretherketone (PEEK) cages and autogenous bone grafts. *J Clin Neurosci* 2008;15:1240–5.
4. Gnecci M, Melo LG. Bone marrow-derived mesenchymal stem cells: isolation, expansion, characterization, viral transduction, and production of conditioned medium. *Methods Mol Biol* 2009;482:281–94.
5. Im BJ, Lee SW, Oh N, et al. Texture direction of combined microgrooves and submicroscale topographies of titanium substrata influence adhesion, proliferation, and differentiation in human primary cells. *Arch Oral Biol* 2012;57:898–905.
6. Fu J, Hu Y, Guo Z, et al. Effect of surface micro-topography of titanium material on the behaviors of rabbit osteoblast in vitro. *Applied Surface Science* 2012;255:286–9.
7. Wang Y, Yu Z, Guo X, et al. Surface morphology of modified titanium alloy affects proliferation stability of bone marrow mesenchymal stem cells. *Surface and Coatings Technology* 2019;366:156–63.
8. Li L, Yang S, Xu L, et al. Nanotopography on titanium promotes osteogenesis via autophagy-mediated signaling between YAP and (-catenin. *Acta Biomaterialia* 2019;96:674–85.
9. Duncan RL, Turner CH. Mechanotransduction and the functional response of bone to mechanical strain. *Calcif Tissue Int* 1995;57:344–58.
10. Golub EE, Boesze-Battaglia K. The role of alkaline phosphatase in mineralization. *Clin Opin Orthop* 2007;18:444–8.
11. Dou X, Wei X, Liu G, et al. Effect of porous tantalum on promoting the osteogenic differentiation of bone marrow mesenchymal stem cells in vitro through the MAPK/ERK signal pathway. *J Orthop Translat* 2019;19:81–93.
12. Janssen S, Gach S, Kant S, et al. Enhanced osteogenic differentiation of human mesenchymal stromal cells as response to periodical microstructured Ti6Al4 V surfaces. *J Biomed Mater Res B Appl Biomater* 2020;108:2218–26.
13. Ninomiya JT, Struve JA, Krolikowski J, et al. Porous ongrowth surfaces alter osteoblast maturation and mineralization. *J Biomed Mater Res A* 2015;103:276–81.
14. Monfoulet LE, Becquart P, Marchat D, et al. The pH in the microenvironment of human mesenchymal stem cells is a critical factor for optimal osteogenesis in tissue-engineered constructs. *Tissue Eng Part A* 2014;20:1827–40.
Cited Here | PubMed | Google Scholar
15. Hofer HR, Tuan RS. Secreted trophic factors of mesenchymal stem cells support neurovascular and musculoskeletal therapies. *Stem Cell Res Ther* 2016;7:131.

Corresponding author:

Joseph L. Laratta, MD,

Department of Orthopedic Surgery, University of Louisville, 550 South Jackson St., 1st Floor Ambulatory Care Building, Louisville, KY 40202;

E-mail: larattaj@gmail.com

Figure 1.

x-Ray micro-CT images of the three-dimensional (3D) titanium (Ti) scaffold demonstrating the randomly distributed, highly porous structure of the scaffold. (A) The scaffold when viewed along the base and height. (B) Oblique view of the scaffold.

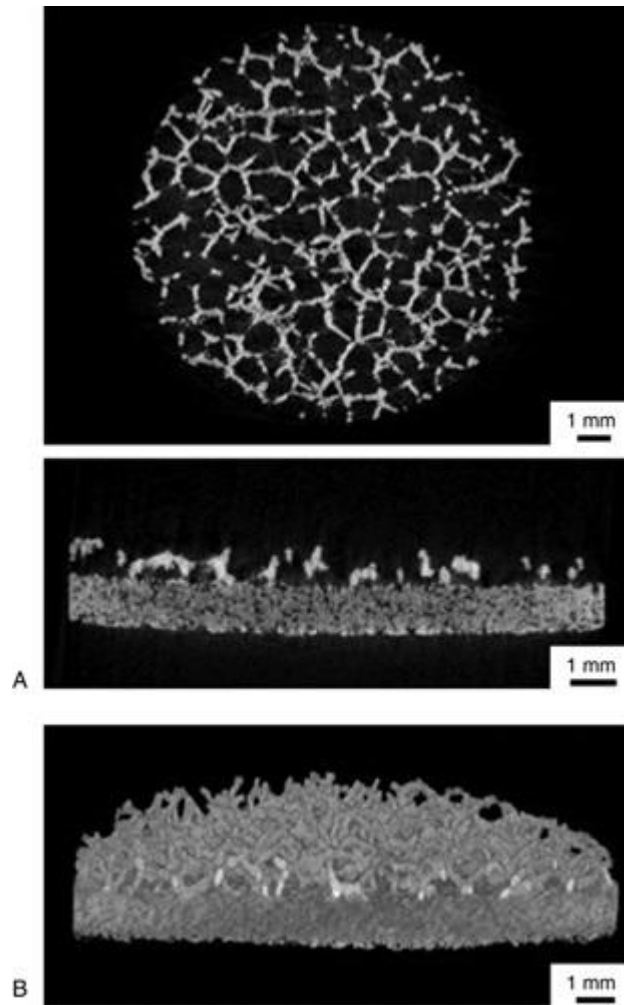


Figure 2.

Scanning electron microscopy images of the two-dimensional (2D) polyetheretherketone (PEEK), 2D titanium (Ti), and 3D-Ti cages demonstrated in Figure 2 display a smooth surface in both the 2D-Ti and 2D-PEEK scaffolds, while a random, textured geometry can be appreciated within the 3D-Ti scaffold. Additionally, the 3D-Ti implant displays spherical depositions of Ti of various size and distribution about the strut surface.

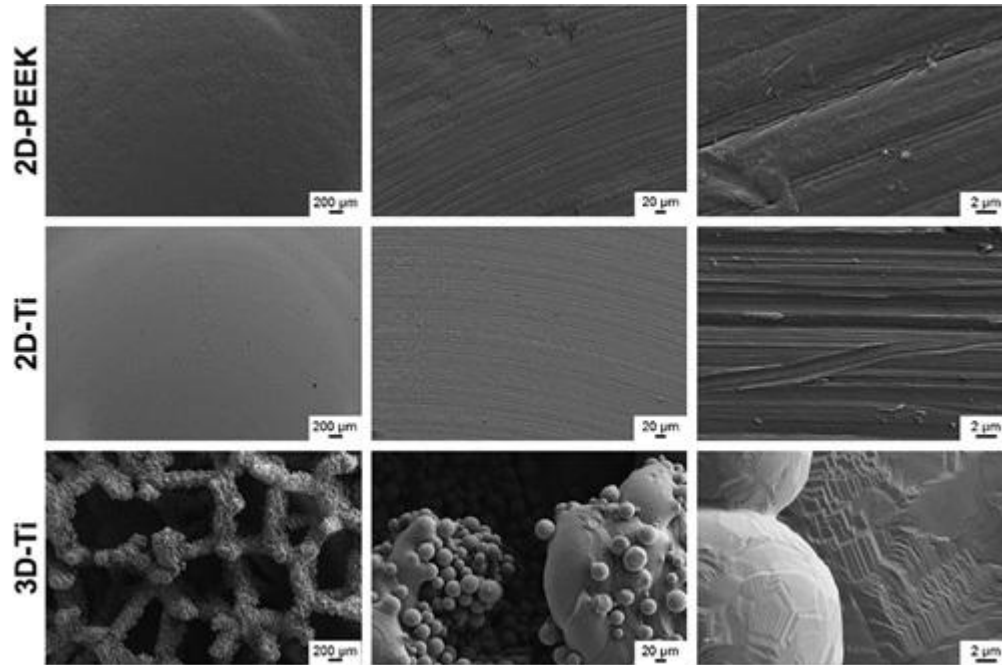


Figure 3.

Confocal images of 3-Dimensional (3D) titanium (Ti) scaffolds after F-actin filaments staining using phalloidin (green) and cell nuclei staining using diamidino-2-phenylindole (blue). (A-C) The scaffold at days 7, 28, and 42 post-seeding of human mesenchymal stem cells (hMSC) scaled at 100 μm . (D-F) The scaffold at 7, 28, and 42 days post-seeding of hMSCs scaled at 25 μm .

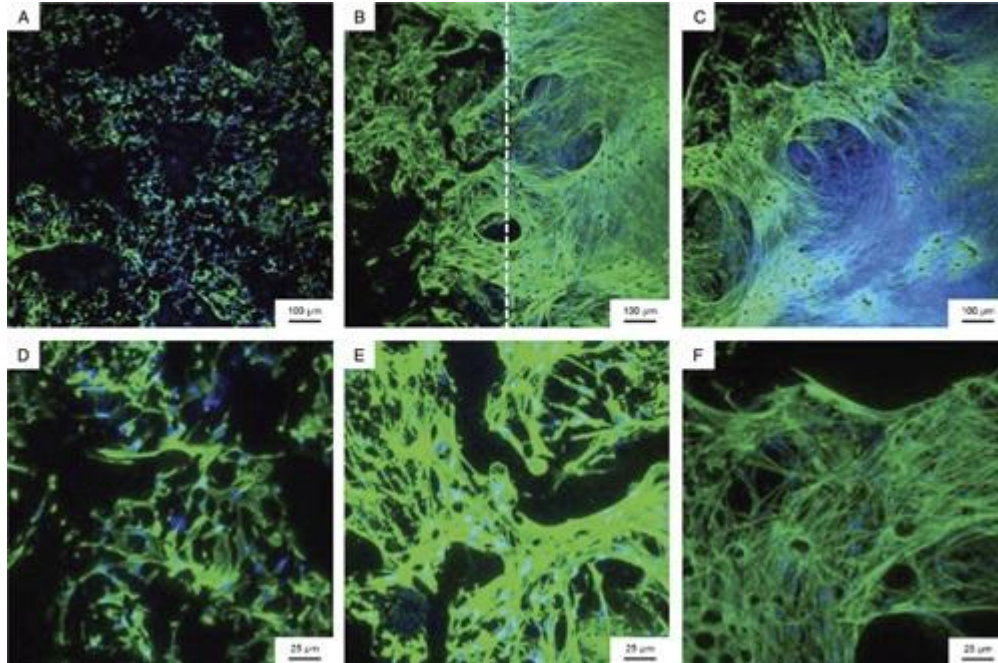


Figure 4.

Environmental scanning electron microscopic images of tissue culture plastic control (TCP), two-dimensional (2D) polyetheretherke-tone (PEEK), 2D titanium (Ti), and 3D Ti scaffolds after 7, 28, and 42 days of experimental treatment. Scaled at 50 μ m.

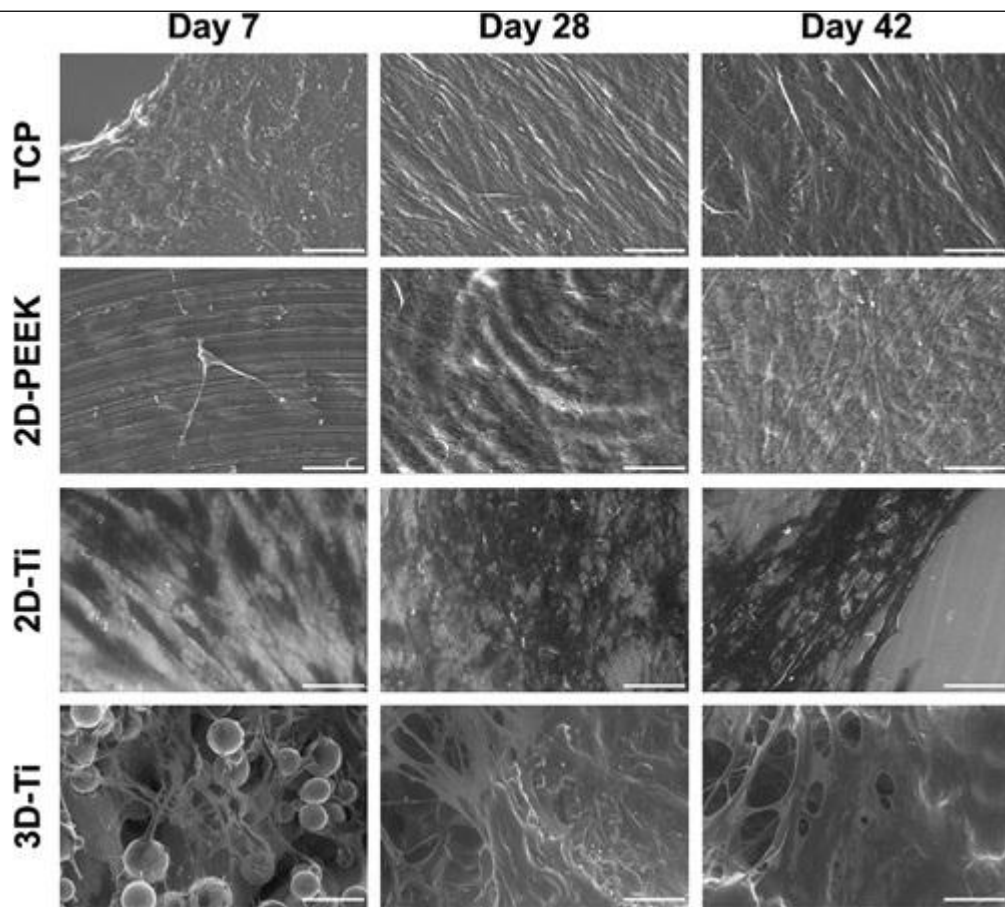


Figure 5.

Cell number per scaffold determined using DNA assay. *Denotes significant P value ($P < 0.05$). (A) tissue culture plastic control (TCP), two-dimensional (2D) polyetheretherketone (PEEK), 2D titanium (Ti), and 3D-Ti scaffolds. (B) 2D-PEEK, 2D-Ti, 3D-Ti compared with one-way analysis of variance with Tukey post hoc analysis test for scaffold effect per time point. Normality of distribution confirmed with Shapiro-Wilk test.

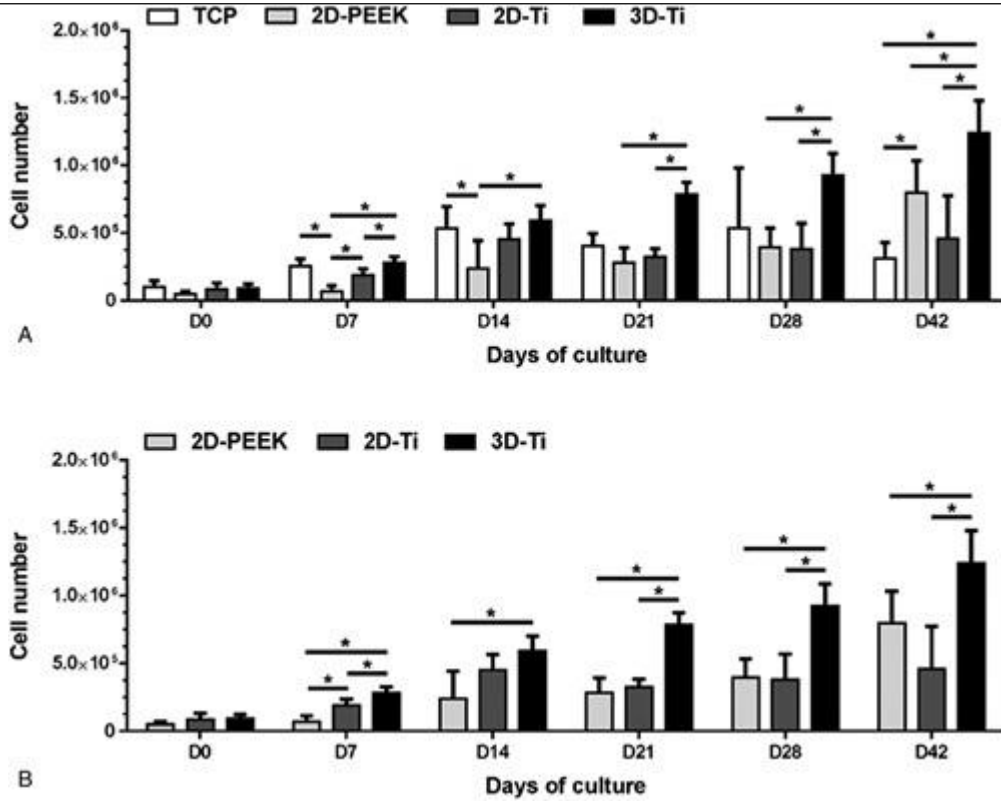


Figure 6.

Human mesenchymal stem cell (hMSC) gene expression levels pertinent to osteogenesis as determined using RT-qPCR. Runt-related transcription factor 2 (RUNX2), Integrin-binding sialoprotein (IBSP), secreted phosphoprotein 1 (SPP1), bone gamma-carboxyglutamic acid-containing protein (bGLAP). * Denotes significant P value ($P < 0.05$). Kruskal-Wallis nonparametric analysis with Bunn post hoc test for scaffold effect per time point, after testing data normality with Shapiro-Wilk test. (A) 2-Dimensional (2D) polyetheretherketone (PEEK), 2D titanium (Ti), and 3D-Ti scaffolds as compared to tissue culture plastic (TCP) controls at 7, 14, 28, and 42 days (D). (B) 3D-Ti, 2D-Ti and 2D-PEEK scaffolds alone at 7, 14, 28, and 42 days.

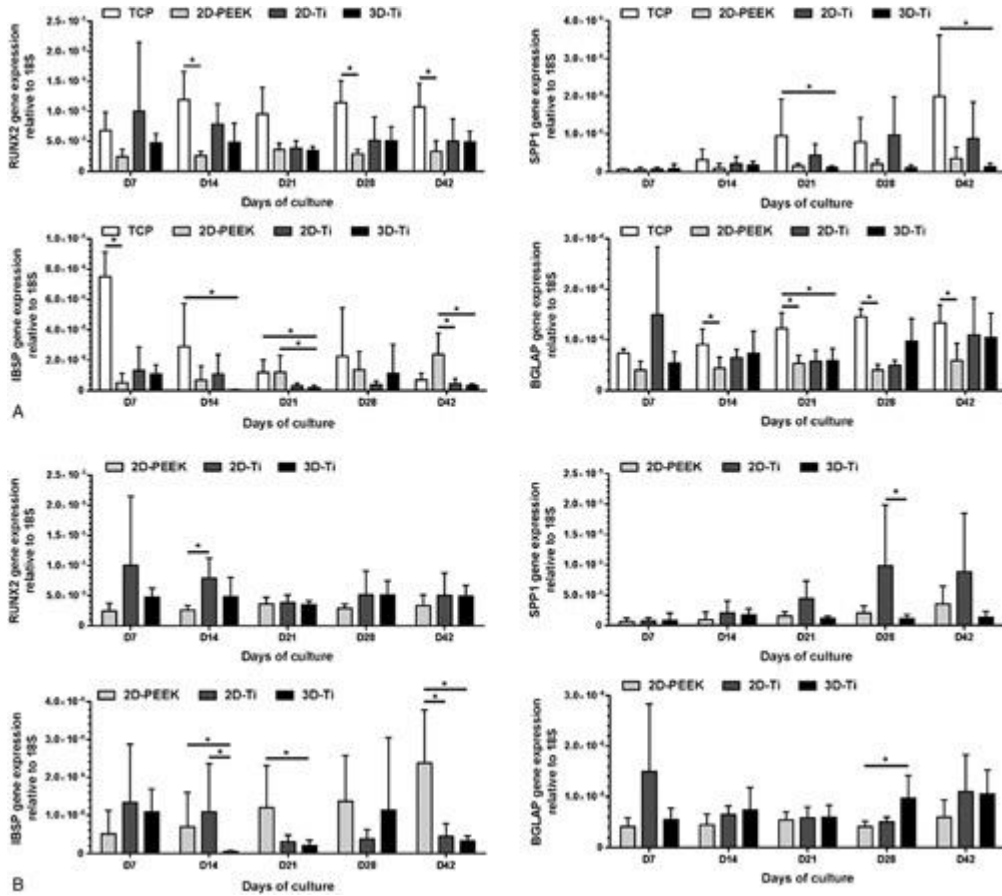


Figure 7.

Alkaline phosphatase (ALP) activity expressed by human mesenchymal stem cell (hMSCs) cultured in osteogenic cell culture medium onto each scaffold and tissue cultured plastic (TCP) controls. *Denotes significant P value ($P < 0.05$). Kruskal-Wallis non-parametric analysis with Bunn's post hoc test for scaffold effect per time point, after testing data normality with Shapiro-Wilke test. (A) Two-dimensional (2D) polyetheretherketone (PEEK), 2D titanium (Ti), and 3D-Ti scaffolds as compared to TCP controls 7, 14, 28, and 42 days (D). (B) 3D-Ti, 2D-Ti and 2D-PEEK scaffolds alone. (C) ALP activity normalized to protein content for 3D-Ti, 2D-Ti and 2D-PEEK scaffolds as compared to TCP controls.

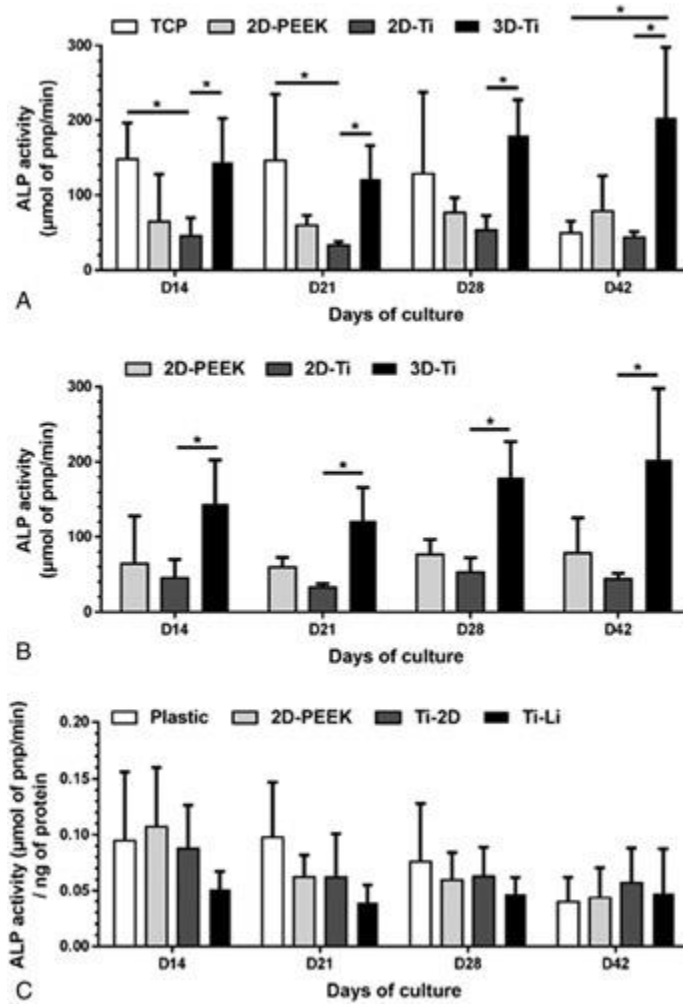


Figure 8.

Calcium content of extra-cellular matrix secreted by human mesenchymal stem cells (hMSCs) cultured in osteogenic cell culture medium onto each scaffolds and tissue cultured plastic (TCP) controls. *Denotes significant P value ($P < 0.05$). One-way ANOVA analysis with Tukey's post hoc test for scaffold effect per time point, after testing data normality with Shapiro-Wilk test. (A) Two-dimensional (2D) polyetheretherketone (PEEK), 2D titanium (Ti), and 3D-Ti scaffolds as compared to TCP controls at day (D) 28 and 42. (B) 3D-Ti, 2D-Ti and 2D-PEEK scaffolds alone. (C) calcium content normalized to cell number for 3D-Ti, 2D-Ti and 2D-PEEK scaffolds as compared to TCP controls.

